ELEVENTH EUROPEAN ROTORCRAFT FORUM

Paper No. 97

THE V-22 TILT-ROTOR LARGE-SCALE ROTOR PERFORMANCE/ WING DOWNLOAD TEST AND COMPARISON WITH THEORY

Michael A. McVeigh
Bell-Boeing
Philadelphia, Pennsylvania, U.S.A.

September 10-13, 1985

London, England.

THE CITY UNIVERSITY, LONDON, EC1V OHB, ENGLAND.

THE V-22 TILT-ROTOR LARGE-SCALE ROTOR PERFORMANCE/ WING DOWNLOAD TEST AND COMPARISON WITH THEORY

Michael A. McVeigh
Bell-Boeing
Philadelphia, Pennsylvania , U.S.A.

Abstract

Rotor performance and wing download data acquired by testing a large-scale model of the rotor and wing for the V-22 multi-mission tilt rotor aircraft is presented. Performance of the rotor was measured in isolation and with a scale model of the V-22 wing in place. The effect of the opposite rotor was simulated by using a large image plane. It was determined that the isolated rotor maximum figure of merit was .808. With the image plane in place, rotor thrust was slightly reduced compared to the isolated rotor value and was caused by the development of a region of recirculating flow near the image plane/wing junction. The wing download and the distribution of the load was determined. With flaps deflected the ratio of download to thrust was 0.093. Comparisons with theory are presented.

Introduction

The V-22 is the multi-mission tilt-rotor aircraft designed for the U.S. Marine Corps, Navy, and Air Force. Since it is a VTOL aircraft, rotor hover performance and wing download are crucial to the achievement of mission requirements. Because of this, during the planning phase of the V-22 program it was decided to take steps to establish, early in the design, the correct levels of rotor figure of merit and wing download. Both small-scale testing and large-scale testing was planned for in the preliminary design stage. At that time, a test of two full-scale, 25-foot diameter rotors was also being planned to take place at the Outdoor Aerodynamic Research Facility (OARF) at NASA-Ames under the Boeing/NASA XV-15 Advanced Technology Blade Program (Refs. 1,2). Accordingly, it was decided to test a 25-foot

diameter model of the 38-foot diameter V-22 rotor (.6579 scale); the same diameter as the XV-15. This rotor, herein referred to as the M901, was large enough to be considered as essentially full scale, requiring only very small corrections to give the performance at the diameter and solidity of the actual V-22 rotor. In addition, back-to-back tests would provide a useful comparison of performance of the three rotors at the same rotor diameter.

Besides obtaining rotor performance data, it was also desired to acquire details on the rotor downwash field and the wing download. A large wake rake was therefore designed to be mounted in the slipstream and the wing was furnished with its own balance system so that the slipstream-induced download could be measured. The wing was also provided with rows of surface pressure taps so that the distribution of download could be determined. This paper describes the test facility and presents the test results together with some comparisons with theory.

Model Description

Test Stand

The test arrangement at the Outdoor Aerodynamic Research Facility (OARF) at NASA-Ames consists of a large concrete pad with a steel platform at the center of which is mounted a test stand carrying the propeller test rig. Fig. 1(a) shows the 25-foot diameter M901 rotor mounted on the Ames 40 x 80 foot wind tunnel propeller test rig. Details of the layout of the stand are given in Fig. 2. The horizontal mounting effectively removes any influence of the ground on rotor performance. The test stand consists of a horizontal frame carrying the motor and drive system. This frame is supported in front by two braced vertical steel beams and, in the rear, by a single smaller beam. The rotor centerline lies 22 feet above the metal platform providing 9.5 feet of clearance between the blade tips and the ground. The rotor hub, controls, six-component balance, gearbox and electric motor with services are mounted in-line within a 28-inch diameter cylindrical cowling. The cowling rests on the horizontal frame and, for this test, was enclosed by a fiberglass fairing representing the general

shape of the V-22 engine nacelle. The motor housing is mounted on three load cells to provide rotor force and moment data that is independent of, and supplemental to, data from the main balance.

Motor and Drive System

The test stand is powered by an electric motor driving through a 4:1 reduction gearbox. The gearbox is oil cooled; the motor is water cooled. Gearbox output shaft torque limit is 252,000 in. lb corresponding to the electric motor limit of 3000 HP at 3000 RPM. This was sufficient to test the rotor to beyond the (scaled) all-engines-operating torque limit. The gearbox unit mounts directly to the face of the motor unit and supports the rotor balance through the balance mounting ring.

Balance

The propeller test stand is furnished with a six-component strain gauge balance. This balance was specially designed for NASA by Boeing under the Boeing/NASA XV-15 ATB Program. As shown in Fig. 3, the rotor balance system is mounted between the hub/stack assembly baseplate and the transmission (through the balance mounting ring). The balance is composed of a front and a rear section. The front section is a multi-flexured, torque-measuring element designed to measure the frictional torque of the rotor drive system. The rear thrust-measuring section of the balance system consists of two flexure plates mounted on either end of cylindrical spacer units. These flexure elements not only measure the thrust load, but also provide data for normal force, side force, pitching moment and yawing moment.

Balance strain gauges are of the foil type and are temperature compensated. The primary sensitivities are in the thrust and torque directions with a maximum error of 50 lb of thrust and 25 in. lb of torque. The balance is designed to withstand the loss of one rotor blade without yielding and has infinite life over the normal operating load range. Load range of thrust is -400 to 16,000 lb and the torque range is 0 to 252,000 in. lb. Total shaft torque is measured by means of a strain-gauged flex coupling at the forward end of the rotor drive shaft which passes through

the center of the balance. The flex coupling is designed to measure a maximum torque of 252,000 in. lb with an accuracy of ± 120 in. lb.

Wing

The wing was a 0.6579-scale reproduction of the V-22 wing, complete with 31% chord full-span flap and follower. A sketch of the wing is shown in Fig. 4. The follower is a short spoiler-like panel hinged at the top of the wing cove. During flight, for flap deflections between 5 and 40 degrees, the follower is deflected 5° trailing edge down permitting normal Fowler action between the flap upper surface and the bottom of the follower. As hover is approached, and the flaps are extended beyond 40 degrees, the follower starts hinging downward so that at 60° flap deflection it touches the upper surface of the flap and remains in contact with it thereafter. This arrangement is intended to provide a smooth path for the impinging rotor downwash from the wing upper surface to the flaps.

The upper and lower surfaces of the main wing and flap, were equipped with pressure taps so that the distribution of the wing download could be determined. The pressure taps were connected to a scanivalve system mounted inside the wing. Fig. 4 shows the location of the pressure taps.

The wing extended downward from the side of the nacelle-like fairing to just above the metal planform of the OARF (see Fig. 2). A 28 ft x 28 ft platform was mounted in the plane corresponding to the aircraft plane of symmetry to provide an aerodynamic image of the rotor and thereby simulate the presence of the opposite rotor on the aircraft. A scaled representation of the aircraft fuselage and wing fairing contours in the neighborhood of the wing root was attached to the wing. The complete wing with fuselage fairing was supported on two struts, each of which was provided with a 6-component balance instrumented to measure wing forces and moments. A photograph of the complete rig with the wing installed is presented in Fig. 1(b).

Hub and Controls

The 3-bladed gimballed rotor hub and upper controls were basic XV-15 rotor components. The M901 blade root attachment was designed to be compatible with this hub. The rotor hub provided control of collective pitch, and longitudinal and lateral pitch. The complete hub/stack assembly was mounted on a base plate (actuator plate) which was also the mounting point for the control actuators and the connecting element to the balance system. A slip ring assembly with 48 rings was incorporated within the stack to provide transmission of data from the rotating components to the data acquisition system. A cowling covered the upper controls and balance and was attached to the motor casing. The cowling provided weather protection and an approximate representation of the V-22 nacelle.

M901 Rotor

The M901 rotor was a three-bladed, 25 ft diameter (0.6579-scale) model of an early design for the 38-ft diameter V-22 rotor and had a thrust-weighted solidity (σ_T) of 0.1138, slightly larger than the current V-22 value of 0.105. The blades were of composite construction and were Mach and dynamically scaled. The blades were instrumented to record flap, lag, and torsional bending moments at selected spanwise positions. Blade chord, twist, airfoil and thickness/chord distributions are given in Fig. 5. The airfoil sections were specially designed and tailored to the tilt rotor operating conditions (Ref. 3). The two-dimensional performance was confirmed by wind tunnel tests.

XV-15 Rotor

The XV-15 blades were the identical flight-worthy blades that had been previously tested by Bell Helicopter Textron Corporation on a whirl tower during the XV-15 development program. The XV-15 rotor has a thrust-weighted solidity of 0.089. The planform; twist, airfoil and thickness/chord distributions are presented in Fig. 6.

Wake Rake and Anemometer

A wake rake consisting of 22 pitot-static tubes was mounted behind the rotor disc plane at the station corresponding to the wing upper surface, .4R. The purpose of the rake was to measure the isolated rotor slipstream velocities under different rotor operating conditions and to use this data to understand the structure of the rotor slipstream and the wing download and its distribution. The wake rake was connected to the same scanivalve system used to measure the wing download pressures.

A wind speed and direction transducer was mounted on a narrow tower and installed near the OARF at approximately 200 feet north and 200 feet east of the rotor hub centerline. The indicator was at the same height above ground as the rotor hub (about 22 feet). The signals from the transducer were fed to the data acquisition equipment in the control room.

Test Procedure

A rigorous calibration of the rotor balance was performed at the place of manufacture before assembly of the propeller test rig at the OARF. Following assembly at Ames, another calibration was made which included checks for thermal drift effects on balance readings and a determination of the interaction between the torque flexure and axial force. The interaction amounted to approximately 4 percent of rotor axial force being carried through the torque flexure. This check calibration showed that the balance was behaving to specifications and that the date obtained from the load cells was in close agreement with the balance data.

The XV-15 blades were installed, checked out and tested. Testing consisted of making repeated sweeps in collective while maintaining zero rotor flapping. Following this testing a new check calibration was made with thrust and torque loads applied singly and in combination. The maximum applied thrust was 7000 lb which corresponds to a rotor $C_T = 0.01$. At this condition the error in rotor thrust was only .10 percent, as read from the balance. The load cell result was 0.4 percent. Various torque levels were then applied at a constant applied thrust of 7000 lb. The maximum balance

error was 0.3 percent at 9000 ft lb of torque (rotor C_p = .0010). The load cell error was 1.4 percent.

The XV-15 blades were removed and the M901 blades installed and tested to determine isolated rotor performance. The image plane was then erected and testing performed to determine the image plane effects. The wing and dummy fuselage were installed and the upper and lower wing balances were check loaded and preliminary runs made to evaluate the wing balance and pressure instrumentation systems. Data on rotor performance and wing download was then obtained with wing flaps deflected. Higher than expected alternating wing balance loads limited the rotor tip speed to 460 fps for the download portion of the test.

Rotor performance in the presence of the wing at full tip speed (installed performance), was obtained with the wing balances locked out. The image plane was removed and performance at full tip speed was measured to determine the partial ground effect of the wing on the rotor.
A final check loading was performed on the rotor balance and the results showed that the accuracy was still within specifications.

Data Reduction

The test program was conducted during the early morning hours when the wind speeds were low, generally less than 3 knots. Because the OARF is situated with the rotor axis pointing north into the prevailing wind, even a wind speed as low as 3 knots will significantly affect rotor performance. A procedure was therefore developed to correct the measured power to the true static conditions using momentum theory.

Except for the wind correction the data reduction procedure was conventional. Data from the rotor balance and load cells was corrected for balance interactions and reduced to coefficient form. The wing pressure data was integrated chordwise and spanwise to give wing forces and the wing balance output processed to give the wing forces as obtained directly from the wing balances.

Results

Isolated Rotor Performance

The variation of power coefficient with thrust coefficient for the isolated M901 rotor at the nominal tip Mach number of .677, is presented in Fig. 7. The rotor was tested with and without the spinner in place and no effect of the spinner is discernable. The variation of rotor figure of merit is shown in Fig. 8. Maximum figure of merit is 0.808 at $C_T/\sigma_T = .135$ and high levels of figure of merit are maintained beyond $C_T/\sigma_T = .11$ up to the maximum C_T/σ_T tested, .16.

The performance of the M901 rotor is compared to that of the XV-15 rotor in Fig. 8 and clearly shows the improved efficiency of the M901 rotor design. From a plot of $C_T^{3/2}$ vs C_p, values of the induced efficiency factor k were calculated and are compared in Fig. 9 to the values for the XV-15 rotor. The values of k for M901 are lower i.e. the rotor is more efficient.

A theoretical estimate of the hover performance of the M901 rotor was made using a lifting-line method and a lifting-surface method. Both methods use the prescribed wake formulations of Kocurek (Ref. 4). Fig. 8 shows that the lifting-line theory underestimates the performance at the peak and that the lifting-surface method predicts the peak well but tends to overestimate the performance at lower thrust coefficients.

Wake Characteristics

The distribution of downwash velocity in the wake of the rotors was measured by a wake rake positioned so that the ends of the probes coincided with the location of the upper surface of the wing. At 75 percent radius, the distance from the rotor disc to the wing upper surface was .40 R. Fig. 10 shows the radial distribution of downwash for the M901 rotor at different thrust coefficients. The shapes suggest that the edge of the inner wake is at 0.2R and that the tip vortex contracts to 0.8R. Peak downwash velocity occurs between .65 and .70R with an essentially linear

variation from .3R to this point. The non-zero values outside the slipstream are attributed to a combination of ambient winds and induction. Also shown in Fig. 10 is the variation of downwash measured on the XV-15 rotor at a C_T = .0105. The shape is typical and may be compared to the M901 distribution at C_T = .0107. The XV-15 downwash velocities are smaller inboard and larger outboard than the M901 rotor for the same thrust. This is the effect of the M901 taper which tends to load up the inner portions of the blade.

In addition to measurements of the wake pressures, a limited series of photographs were obtained of the tip vortices on the XV-15 blade which were made visible by water vapor condensation. The insert to Fig. 11 is a typical example and shows clearly the helical path of the vortices from each blade. By measuring from these photographs, M. Maisel of NASA Ames succeeded in constructing the shape of the outer wake (see Ref. 5). Fig. 11 shows that at 0.4R downstream, the tip vortex is located at 0.80R. This value is confirmed by the downwash data of Fig. 10.

Installed M901 Rotor Performance

The complete installed rotor performance (i.e. the performance with the wing in place and the effect of the other rotor simulated by the image plane) is presented in Fig. 12. Comparing a faired line through this data to the isolated rotor performance, there is a reduction in thrust for a given power. The reduction varies from 1.8 percent at a C_p = .0009 to 1.2 percent at C_p = .0016. Also shown is the performance of the rotor with the wing present but with the image plane removed. The partial ground effect of the wing on the rotor increases the rotor thrust for a given power. At C_p = .0016 the increase is about 2.7 percent. Fig. 13 indicates that this is in agreement with Cassarino's data (Ref. 6) on the thrust of single rotors operating in the presence of wings or fuselages.

The installed rotor figure of merit is presented in Fig. 14 and shows that there is a reduction in peak figure of merit compared to the isolated rotor. At C_T = .016 the installed figure of merit is 0.793 vs 0.808

isolated. Also, beyond C_T = .016 the figure of merit falls off more rapidly than that of the isolated rotor.

The reduction in performance caused by the wing and image is attributed to the existence of a region of recirculating flow between the wing and the rotor. This pattern was observed during the test and was made visible using tufts and colored smoke. The principal features of the flow pattern are illustrated in Fig. 15. The downwash that impinges on the wing flows radially outward from the rotor centerline. Most of this downwash reaches the edge of the wing where it joins the main flow from the rotor. The surface flow that lies within the sector OAB meets the flow from the opposite rotor, rises, and is then entrained by the rotor thereby setting up a closed region of recirculating flow. The insert to Fig. 15 shows the flow pattern computed using VSAERO (Ref. 7). This pattern and the OARF observations are confirmed by flow visualization studies conducted on the XV-15 aircraft and on a powered wind tunnel model of the V-22.

Full Scale Performance

The performance of the isolated full-scale 38-foot diameter M901 rotor was estimated based on the 25-foot M901 rotor results. The correction method used (Ref. 8) accounts for the effect of Reynolds number on airfoil section lift and drag as well as chord and diameter changes. Fig. 14 presents the estimated full-scale performance of the isolated rotor at 38-foot diameter. The effects of scale are small enough that the large-scale performance is practically the same as full scale.

Download

All of the download data from the wing balance was acquired at reduced tip speed, 460 fps, due to limitations on the wing balance. Consequently, the forces acting on the wing were less than those at full tip speed because the thrust and therefore the downwash velocities were lower. However, as shown in Appendix A, the ratio of the download to the thrust should be

independent of tip speed provided that there are no significant Reynolds number effects present. For a bluff body like the wing, the Reynolds number in the rotor downwash at full tip speed is about 4.2×10^6, based on the wing chord. At the reduced tip speed, the Reynolds number is 2.4×10^6. Within this range of Reynolds number no change in wing drag coefficient would be expected and therefore the values of download/thrust obtained at the reduced tip speed should be the same as those at full tip speed.

In addition to the wing balance data, download was also calculated independently using the measured pressure distributions. Pressure distributions were recorded at full scale tip speed as well as at the reduced tip speed.

The ratio of wing download to rotor thrust with flap set to 67 degrees is plotted versus rotor thrust coefficient in Fig. 16. Some data scatter exists, but the general trends and levels are clear. The download/thrust decreases slightly with increasing thrust coefficient; at very low values of C_T the ratio is slightly greater than 10 percent and at high values, the ratio is about 9 percent. At a nominal design C_T of 0.016, the download-to-thrust ratio is 9.3 percent.

The balance data of Fig. 16 was acquired at reduced tip speed. However, wing pressure data was obtained at full tip speed. Fig. 17 is a typical plot of the chordwise pressure distribution over the main wing and flap at r/R = .30 and full tip speed. At this flap setting, the main wing is producing download whereas the flap is experiencing an upper surface suction which gives a small lifting force, tending to reduce the download. The flow over the flap also creates a rearward force which will require the application of small amounts of forward disc tilt to trim the aircraft. Fig. 18 presents the spanwise loading obtained from this data at three values of rotor thrust coefficient. The loadings were extrapolated (dashed lines) in the regions where no pressure taps were available and integrated to yield a total download. The corresponding values of download/thrust are plotted in Fig. 16 and show reasonable agreement with the wing balance data at the reduced tip speed. It is therefore concluded that download/thrust ratio is independent of tip speed. The simple analysis presented in Appendix A confirms this observation and shows that the ratio of download to

thrust depends on the radius of the contracted slipstream and on the shape of the rotor slipstream velocity distribution. As the downwash changes from nearly uniform at low thrust to skewed toward the tip at high thrust, the download/thrust decreases. Based on the measured slipstream velocities, values of download/thrust were calculated using the theory and are compared to the test values in Fig. 16. Good agreement is achieved considering the simplicity of the approach.

The effect of flap deflection on download is presented in Fig. 19 as a plot of download/thrust ratio versus flap deflection. The measured OARF download values are compared to download levels deduced from flight tests of the XV-15 aircraft. The comparison is favorable and indicates that 67° is likely to be the flap setting giving the lowest download.

Conclusions

Tests of a large-scale rotor model similar to the V-22 rotor and wing demonstrated exceptional accuracy and repeatability for rotor performance data. A maximum figure of merit of .808 was measured for the isolated rotor. With the wing in place and the presence of the opposite rotor on the airplane simulated by an image plane, the figure of merit decreased slightly to .794 due to the establishment of a region of recirculating flow between the rotor and the wing.

With flaps set to 67 degrees, the ratio of wing download to rotor thrust at the operating condition was 0.093. Download/thrust was found to be independent of tip speed and reduced slightly with increasing rotor thrust coefficient. The measured levels of download are similar to values obtained from flight tests of the XV-15 aircraft.

References

1. McVeigh, M. A.; Rosenstein, H.; and McHugh, F. J., Aerodynamic Design of the XV-15 Advanced Composite Tilt Rotor Blade, AHS Forum, May 1983.

2. Smith, K. E.; Alexander, H.; and Maisel, M.; Design Aspects of the XV-15 Advanced Technology Blade Program, AHS Forum, 1985.

3. Narramore, J.; Advanced Technology Airfoil Development for the XV-15 Tilt Rotor Vehicle, AIAA/NASA-Ames V/STOL Conference, December 1981.

4. Kocurek, J. D., and Tangler, J. L.; A Prescribed Wake Lifting Surface Hover Performance Analysis, AHS Forum, 1976.

5. Alexander, H.; Maisel, M.; and Giulianetti, D.; The Development of Advanced Technology Blades for Tilt Rotor Aircraft, Eleventh European Rotorcraft Forum, September 1985.

6. Cassarino, S. J.; Effect of Rotor Blade Root Cutout on Vertical Drag USAAVLABS Tech Report 70-59, October 1970.

7. Clark, D. R.; Analysis of the Wing/Rotor and Rotor/Rotor Interactions Present in Tilt-Rotor Aircraft, Paper presented at the International Conference on Rotorcraft Basic Research, ARO, Dunham, N.C., February 1985.

8. Keys, C. N.; McVeigh M. A.; Dadone, L.; McHugh, F. J.; Considerations in the Estimation of Full-Scale Rotor Performance from Model Rotor Test Data, AHS Forum, 1983.

APPENDIX A: Approximate Calculation of Download and Thrust Loss

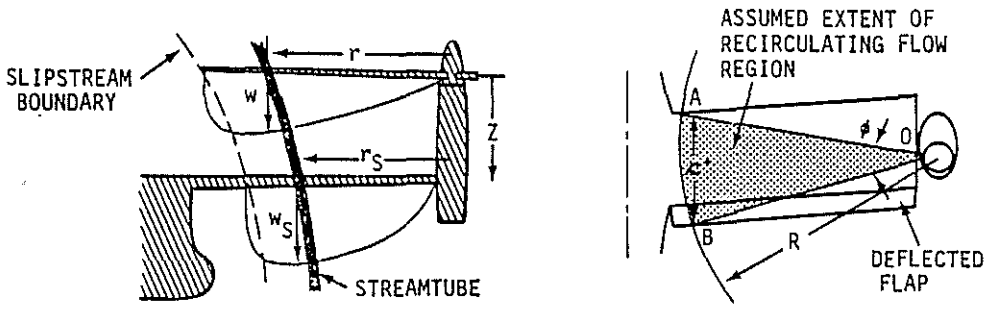

Download

Referring to the sketch, the download on one wing panel is

$$DL = \tfrac{1}{2}\rho \int_0^{R_s} w_s^2 \, c C_d \, dr_s \qquad (1)$$

where C_d is the section drag coefficient based on the flaps-up chord c. From continuity, along a streamline,

$$w_s r_s dr_s = w r dr \qquad (2)$$

where the velocities w and w_s both vary with radial position. Assuming that the slipstream contraction occurs such that $w_s(r_s)$ is always proportional to w(r) i.e.

$$\frac{w_s}{w} = \frac{r dr}{r_s dr_s} = f(z) \text{ only} \qquad (3)$$

then integrating (3)

$$\frac{w_s}{w} = \frac{r^2}{r_s^2} = \frac{R^2}{R_s^2} \qquad (4)$$

Using (2) and (4) in (1)

$$DL = \tfrac{1}{2}\rho \frac{R^3}{R_s^3} \int_0^R c \, C_d \, w^2 dr \qquad (5)$$

Thrust

The elementary rotor thrust is

$$dT = \rho w w_s r dr d\psi \qquad (6)$$

and this is integrated over all of the disc except the recirculating flow region assumed to be the sector OAB. The total thrust is then

$$T = \rho(2\pi-\phi) \int_0^R w w_s r dr \tag{7}$$

where the angle ϕ is given approximately by

$$\phi = c'/R \qquad \text{where } c' \text{ is the projected chord.} \tag{8}$$

Using (2) in (7) the installed value of rotor thrust is

$$T = \rho(2\pi-\phi)\, R^2/R_s^2 \int_0^R w^2 r dr \tag{9}$$

The induced velocity at the disc may be expressed in the form

$$w^2 = V_T^2 \sum_0^\infty a_n x^n \tag{10}$$

where V_T is the tipspeed, $x = r/R$, and a_n are coefficients. Using (10) in (9) and (5), the ratio of download to thrust becomes

$$\frac{DL}{T} = \frac{c}{D}\frac{R}{R_s}\frac{C_d}{(2\pi-\phi)} \frac{\sum_0^\infty a_n/n+1}{\sum_0^\infty a_n/n+2}$$

$$= \frac{c}{R}\frac{R}{R_s}\frac{C_d}{(2\pi-\phi)}\left[\frac{1 + \frac{1}{2}\frac{a_1}{a_0} + \frac{1}{3}\frac{a_2}{a_0} + \cdots}{1 + \frac{2}{3}\frac{a_1}{a_0} + \frac{1}{2}\frac{a_2}{a_0} + \cdots}\right] \tag{11}$$

This shows that the download/thrust does not depend on the tip speed but is a function of the shape of the downwash distribution and the slipstream contraction. From Fig. 10 the shape of the downwash, which depends on blade twist, varies with thrust coefficient; however, the contraction of the slipstream is only weakly dependent on C_T. Note that uniform downwash ($a_n = 0$, $n \geq 1$) does not result in minimum download/thrust.

Using the measured values of downwash (Fig. 10) and assuming that the downwash at the disc is also nearly linear, values of the coefficients a_n

were calculated. A value of C_d=1.12 for flaps set to 67 degrees was obtained from in-house wind tunnel tests. With R_s/R =.8, equation (11) was used to calculate the download and the results are plotted in Fig. 16. The agreement with test data is very good considering the simplicity of the method. This probably means that whereas the individual values of download and thrust may not be predicted well by the simple analysis, the ratios agree with test data because the same method is used to estimate each.

Thrust Loss

The induced power required for a given thrust T is

$$P_i = \int_0^{2\pi-\phi} \int_0^R \rho w^2 w_s r dr d\psi$$

$$= \rho(2\pi-\phi) \frac{R^2}{R_s^2} \int_0^R w^3 \, r dr \qquad (12)$$

If we assume that the rotor profile power is unchanged whether the rotor is isolated or in the presence of the wing then, for a given value of total power, the induced powers are equal i.e.

$$(2\pi-\phi) \int_0^R w^3 r dr = 2\pi \int_0^R w_\infty^3 \, r dr \qquad (13)$$

For uniform downwash the induced power is

$$P_i = Tw = T_\infty w_\infty \qquad (14)$$

and the fractional thrust loss is, using (13),

$$\frac{T}{T_\infty} = \frac{w_\infty}{w} = \sqrt[3]{1-\phi/2\pi} \qquad (15)$$

For the V-22 model, ϕ = .372, and T/T_∞ = .98 i.e. a 2% loss. From Fig. 10 the downwash is nearly uniform at C_T = .0107 and from Fig. 12 the measured thrust loss is 1.8 percent at this value of C_T, which agrees well with the simple analysis.

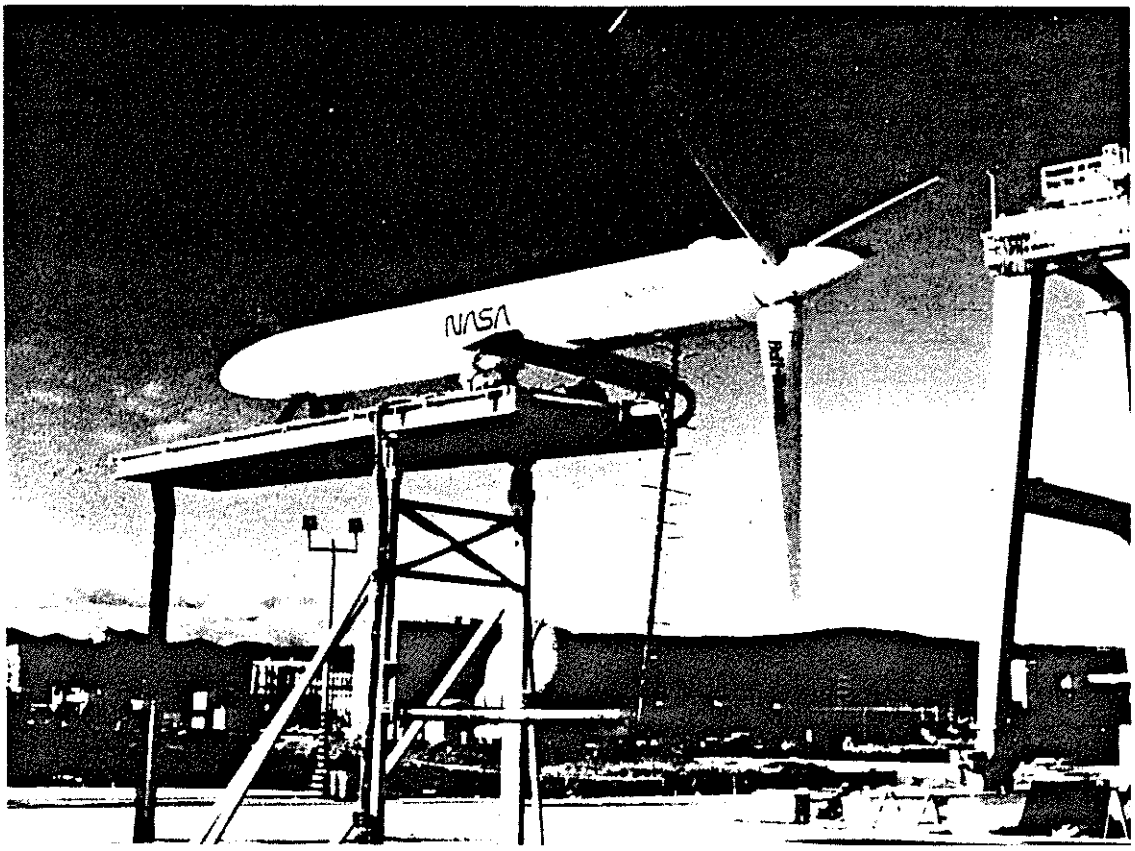

Fig. 1(a). M901 Rotor on Propeller Test Stand

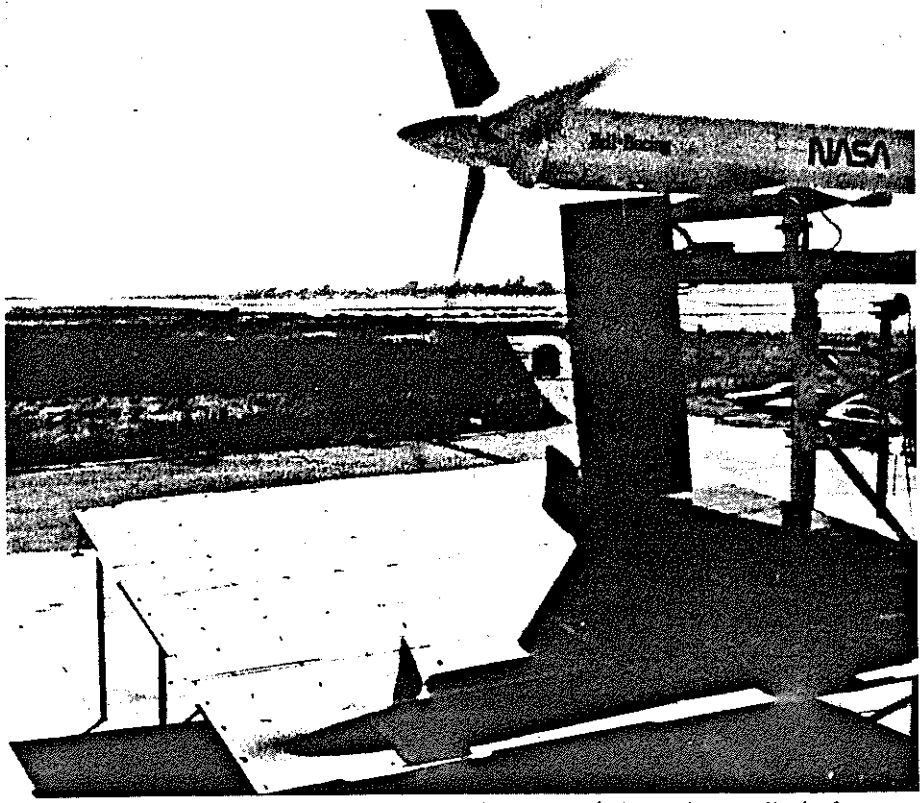

Fig. 1(b). M901 Rotor, Wing, and Fuselage Fairing on Propeller Test Stand

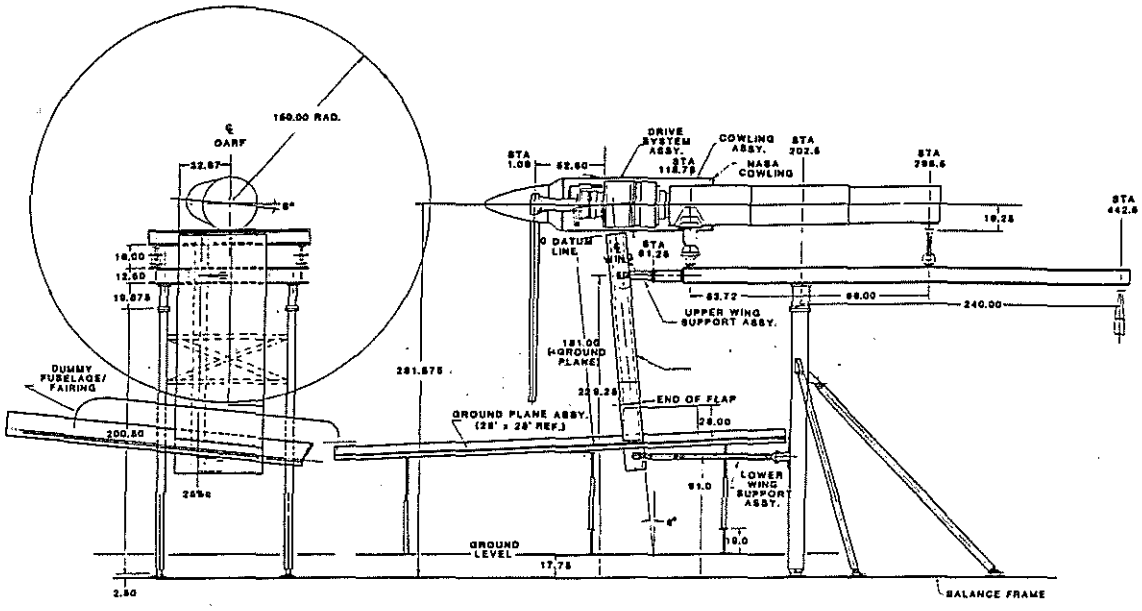

Fig. 2. Test Stand Layout

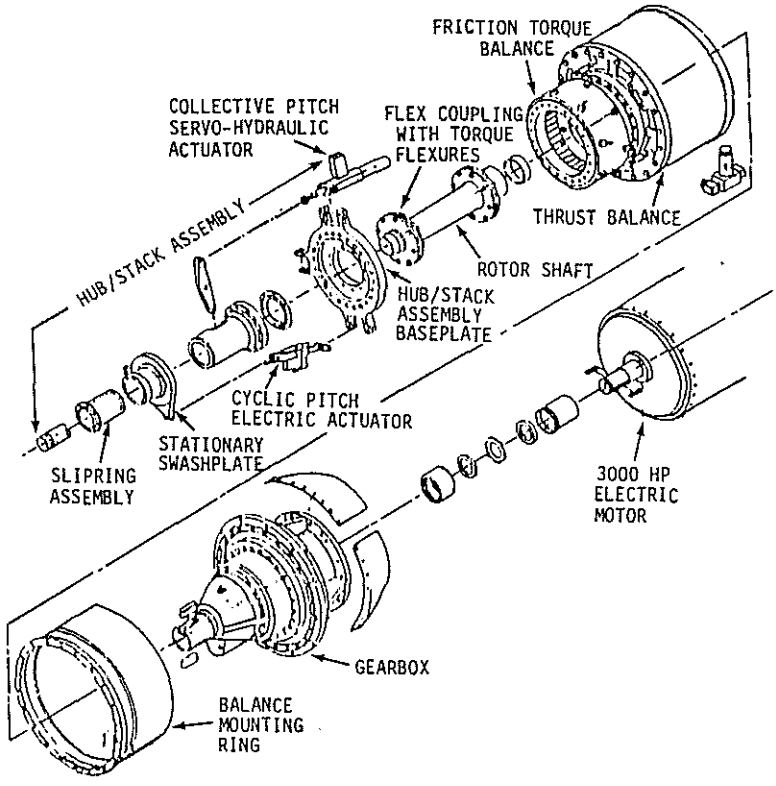

Fig. 3. Details of Propeller Test Stand, Hub, Balance, and Drive System

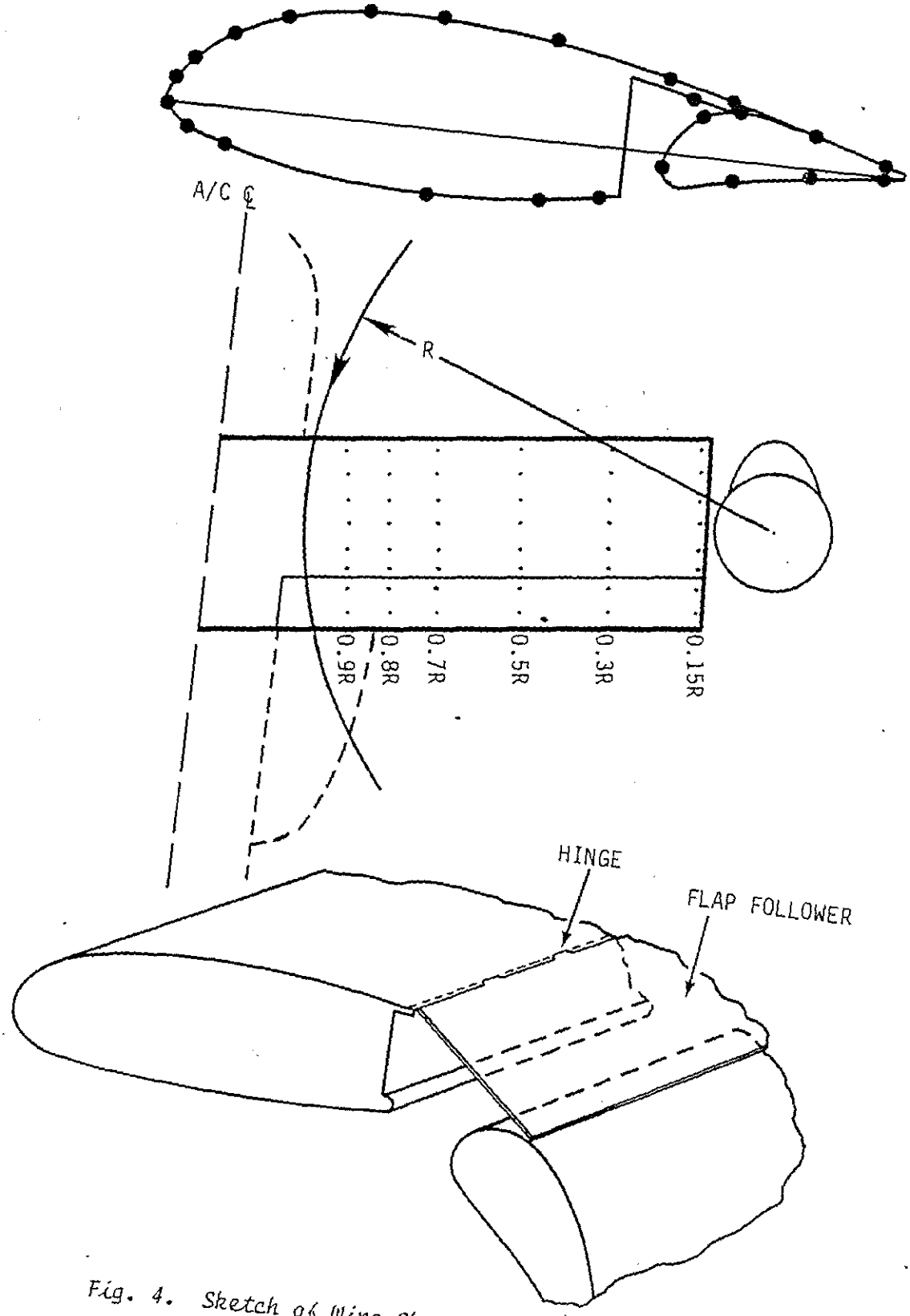

Fig. 4. Sketch of Wing Showing Pressure Taps and Flap and Follower Arrangement

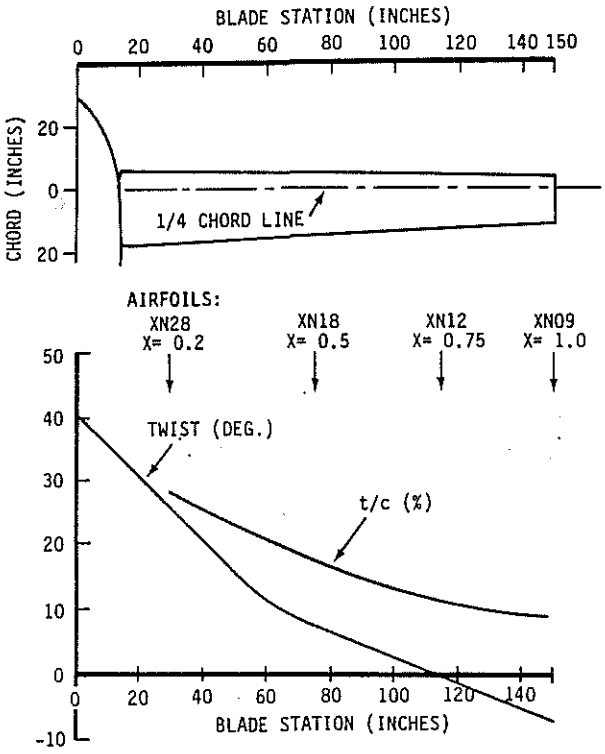

Fig. 5. Geometry of M901 Rotor Blade

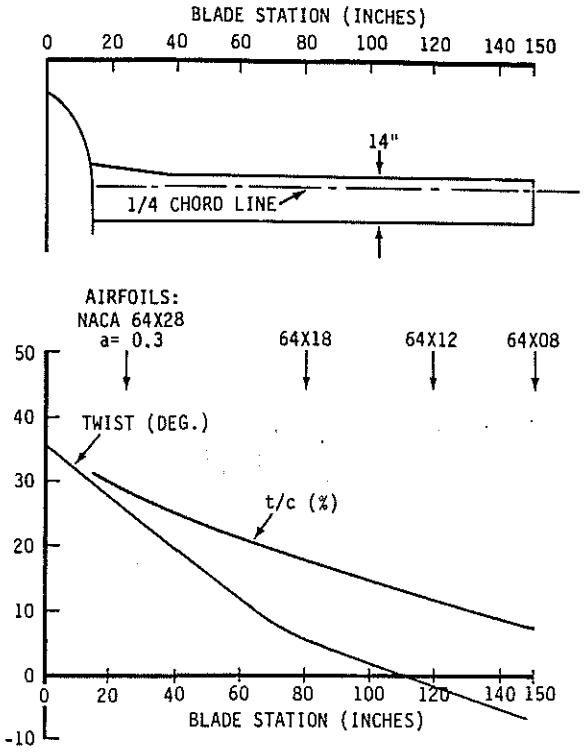

Fig. 6. Geometry of XV-15 Rotor Blade

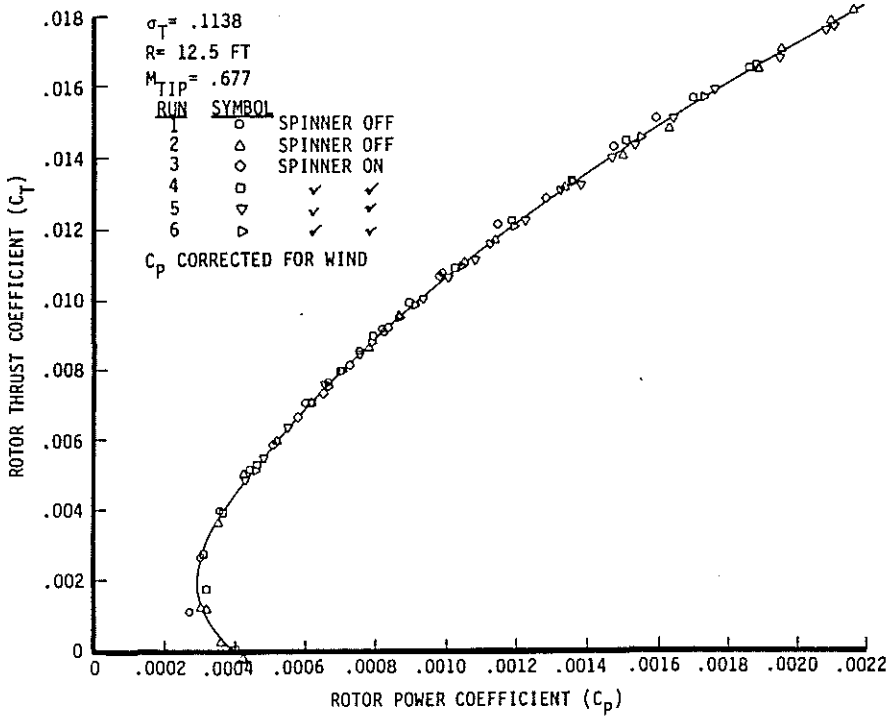

Fig. 7. C_T vs. C_p for Isolated M901 Rotor

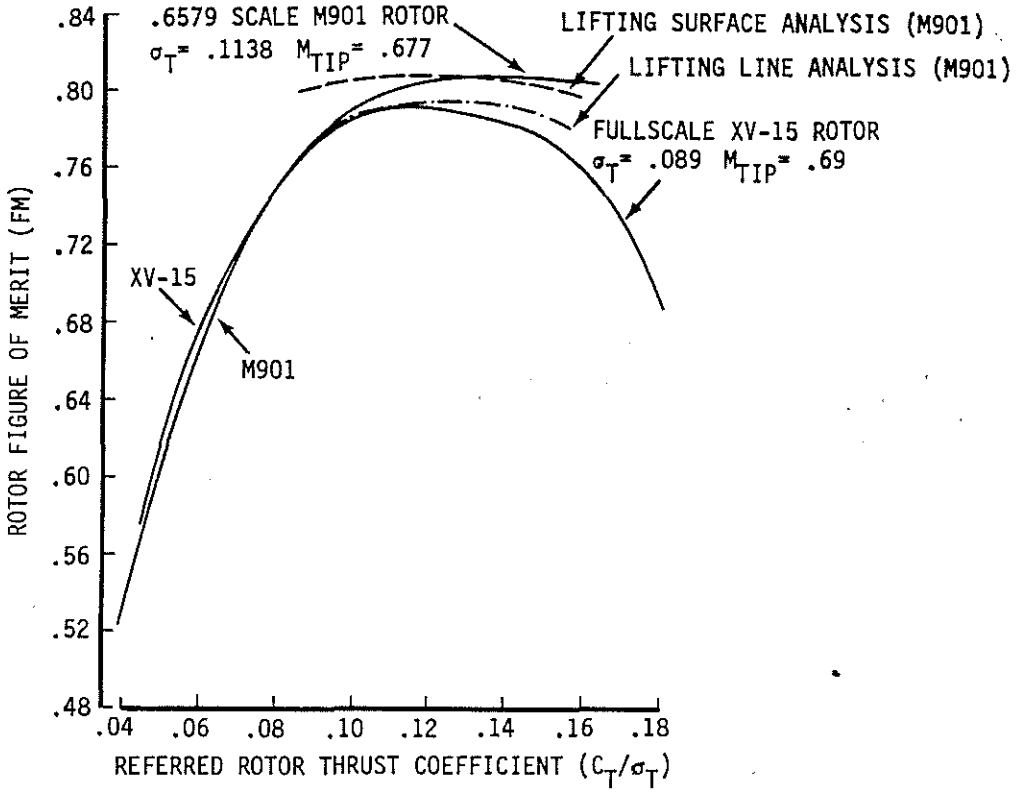

Fig. 8. Performance of the Isolated M901 and XV-15 Rotors and Comparison with Theory

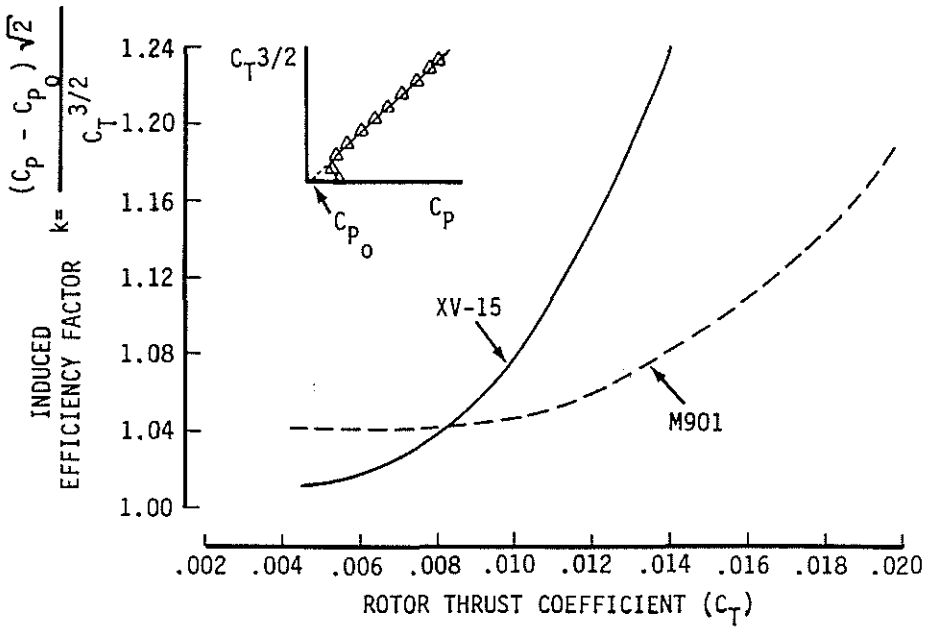

Fig. 9. Variation of Induced Efficiency Factor with Thrust Coefficient for XV-15 and M901 Rotors

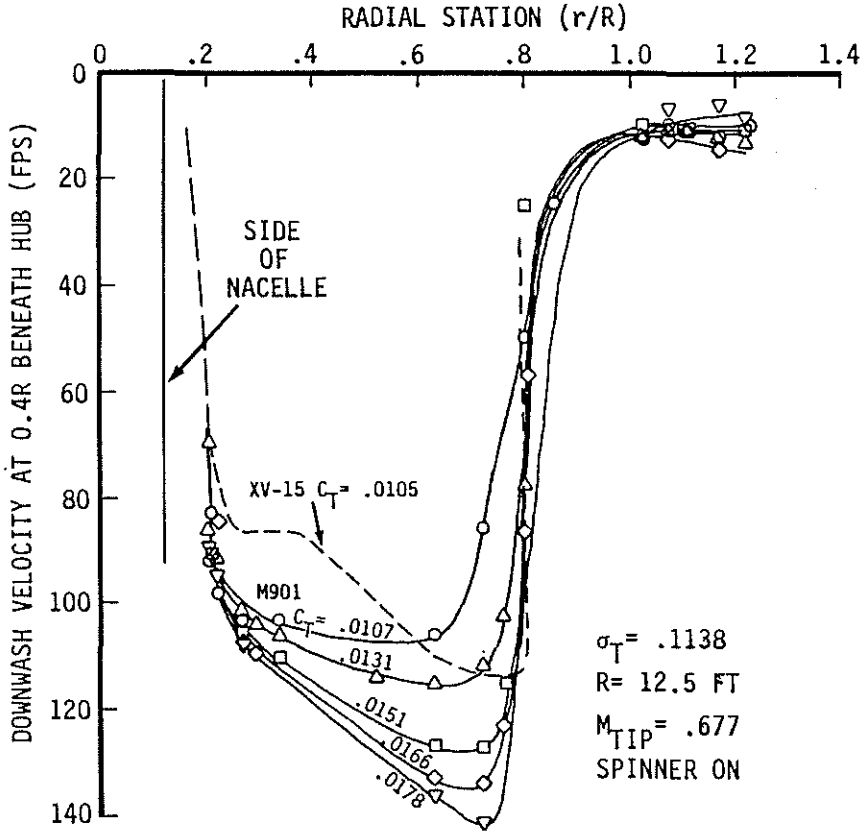

Fig. 10. *Downwash Distribution Beneath the Isolated M901 and XV-15 Rotors*

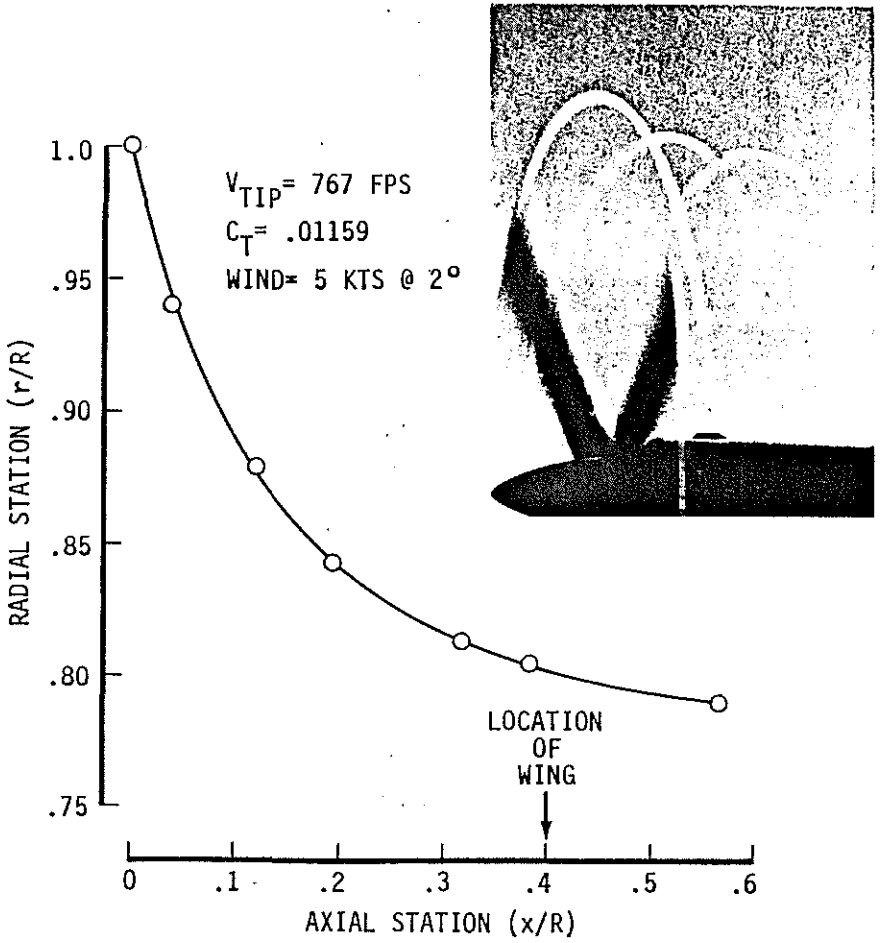

Fig. 11. *Wake Shape of XV-15 Rotor Deduced from Tip Vortex Photographs*

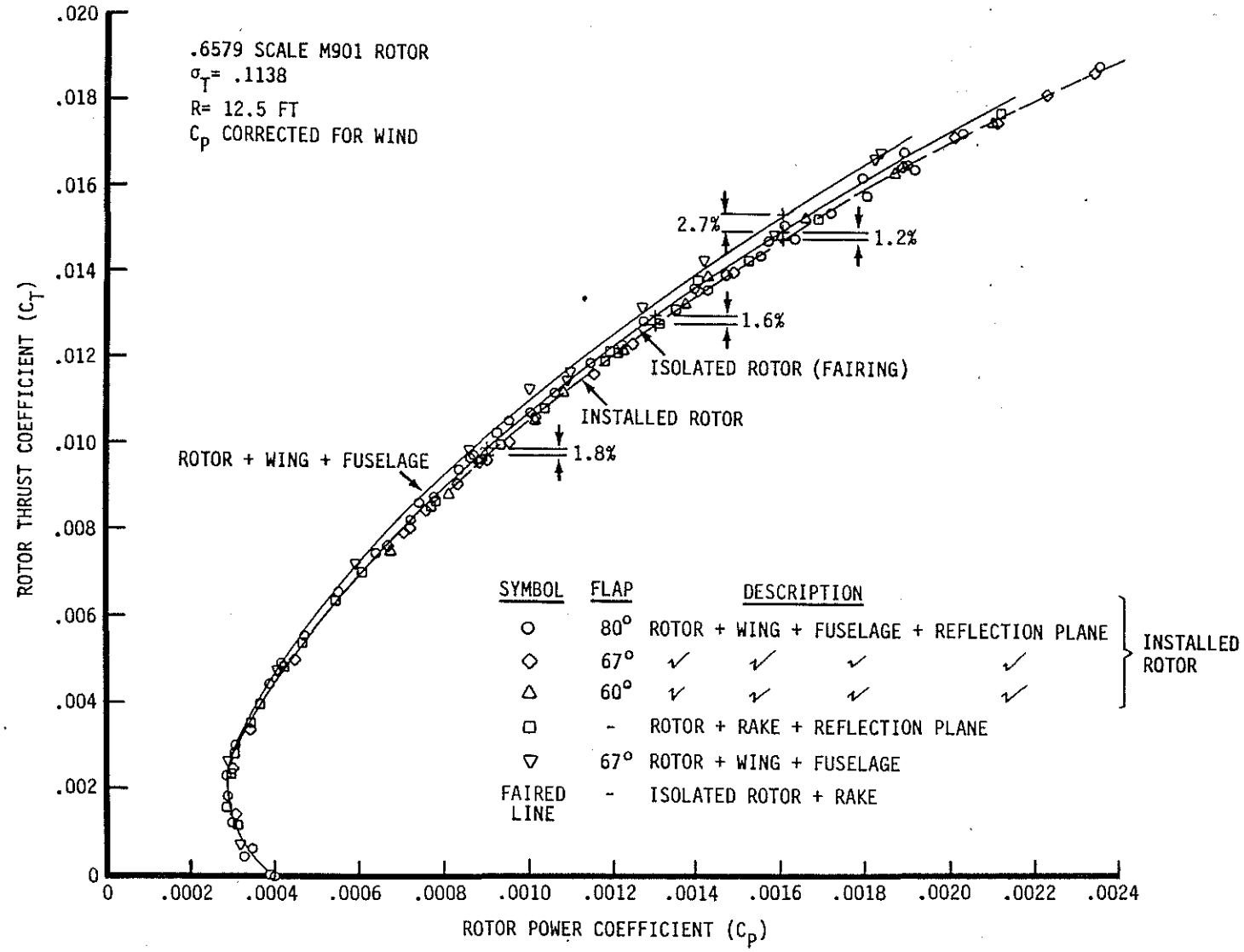

Fig. 12. Installed Performance of the Large-Scale M901 Rotor

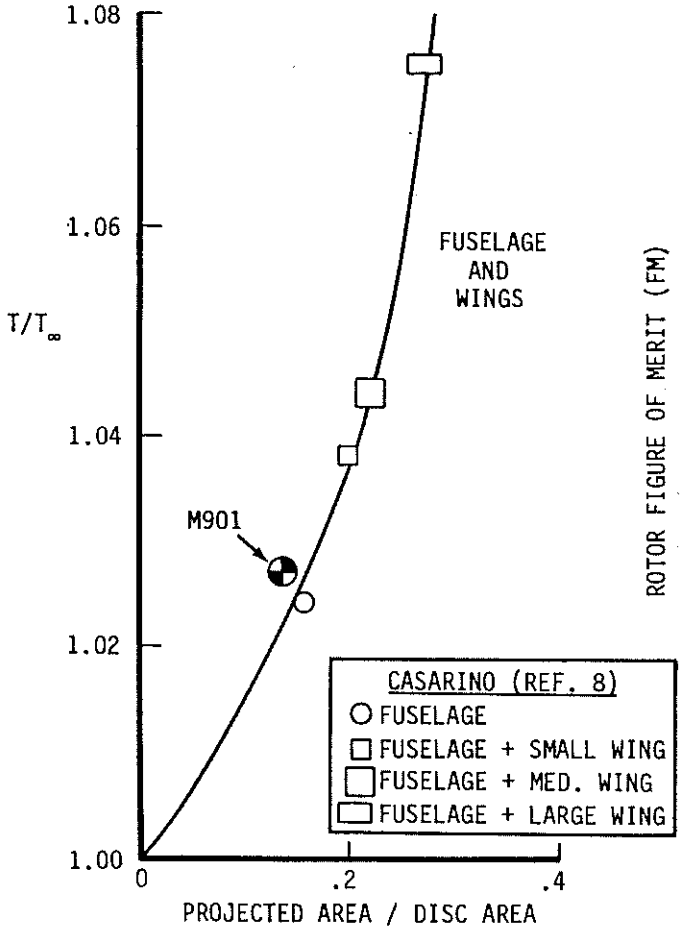

Fig. 13. M901 Rotor Thrust Recovery - Comparison with Other Data

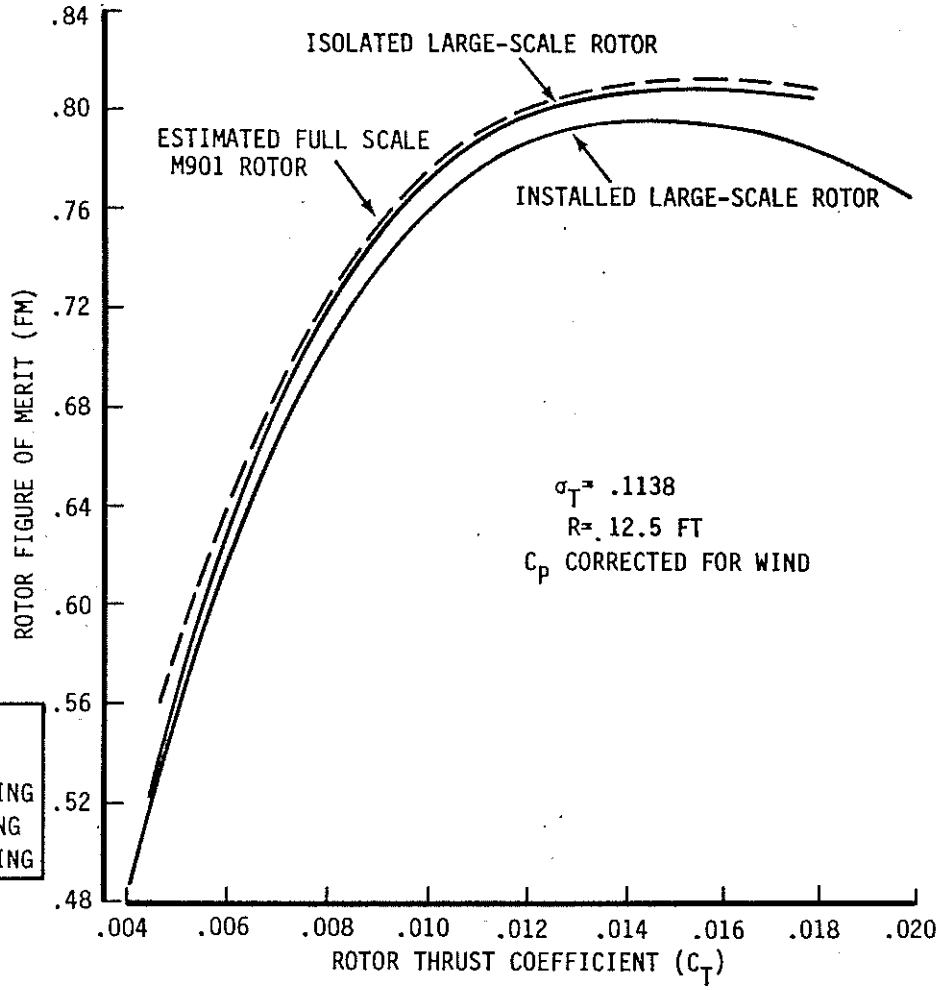

Fig. 14. Installed Rotor Performance for M901 Rotor

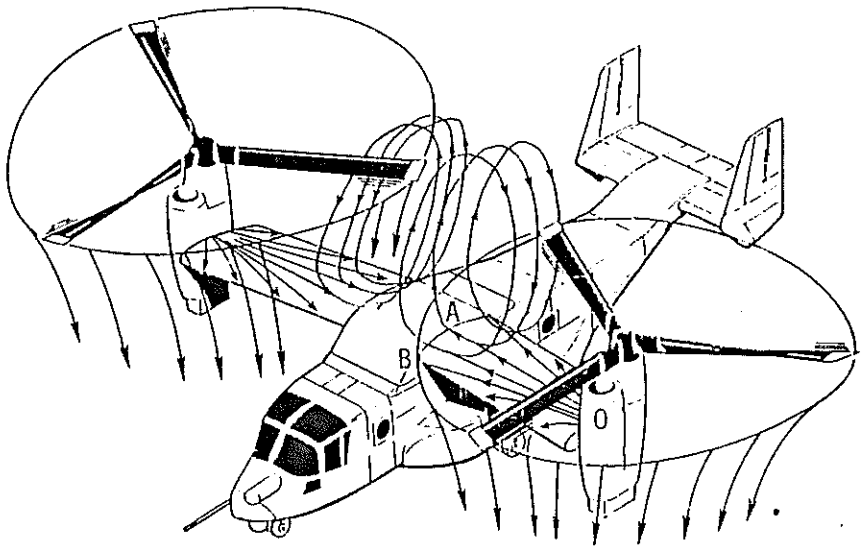

OBSERVED

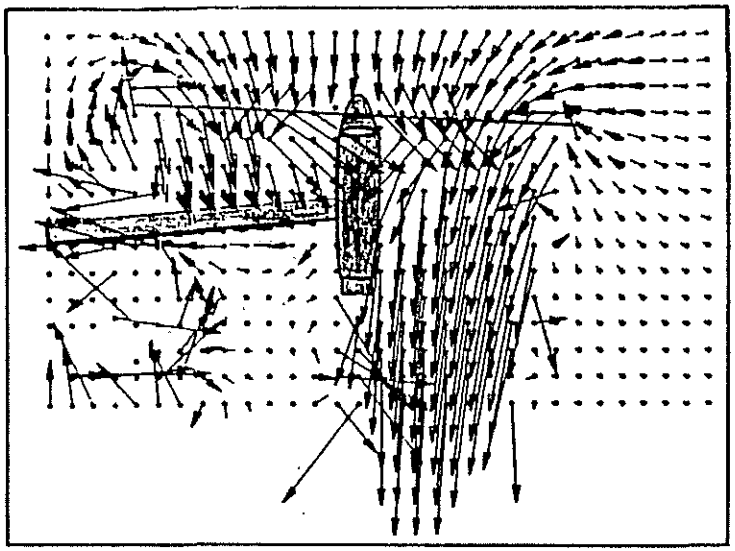

COMPUTED USING VSAERO

Fig. 15. Wing/Rotor Flow Pattern in Hover

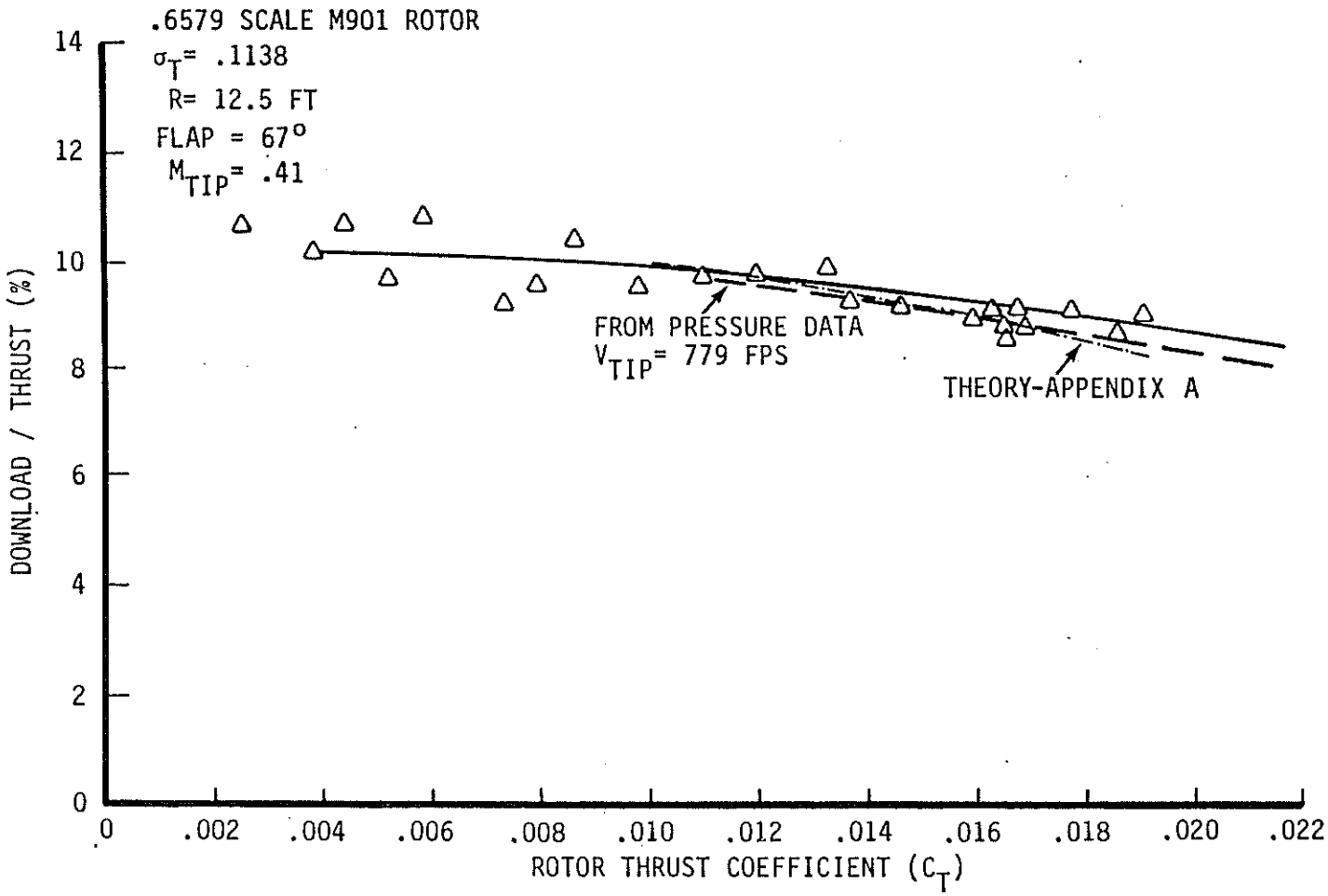

Fig. 16. Variation of Wing Download/Thrust with Rotor Thrust Coefficient

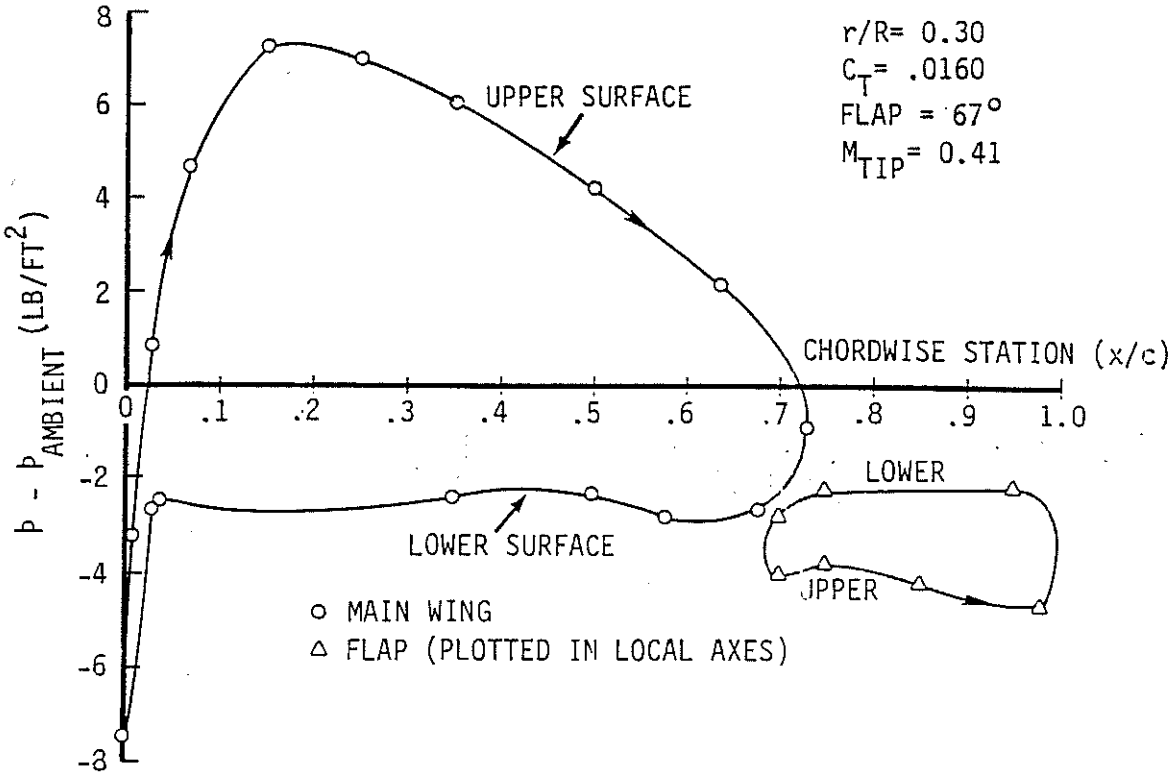

Fig. 17. Chordwise Pressure Distribution

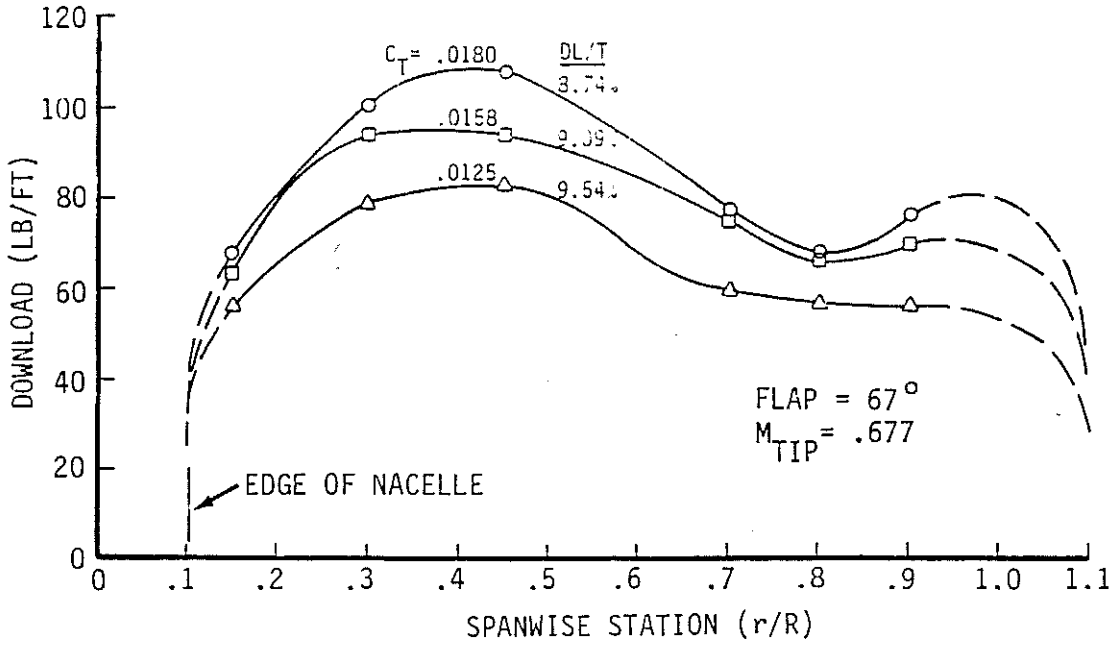

Fig. 18. Spanwise Distribution of Download from Pressure Taps

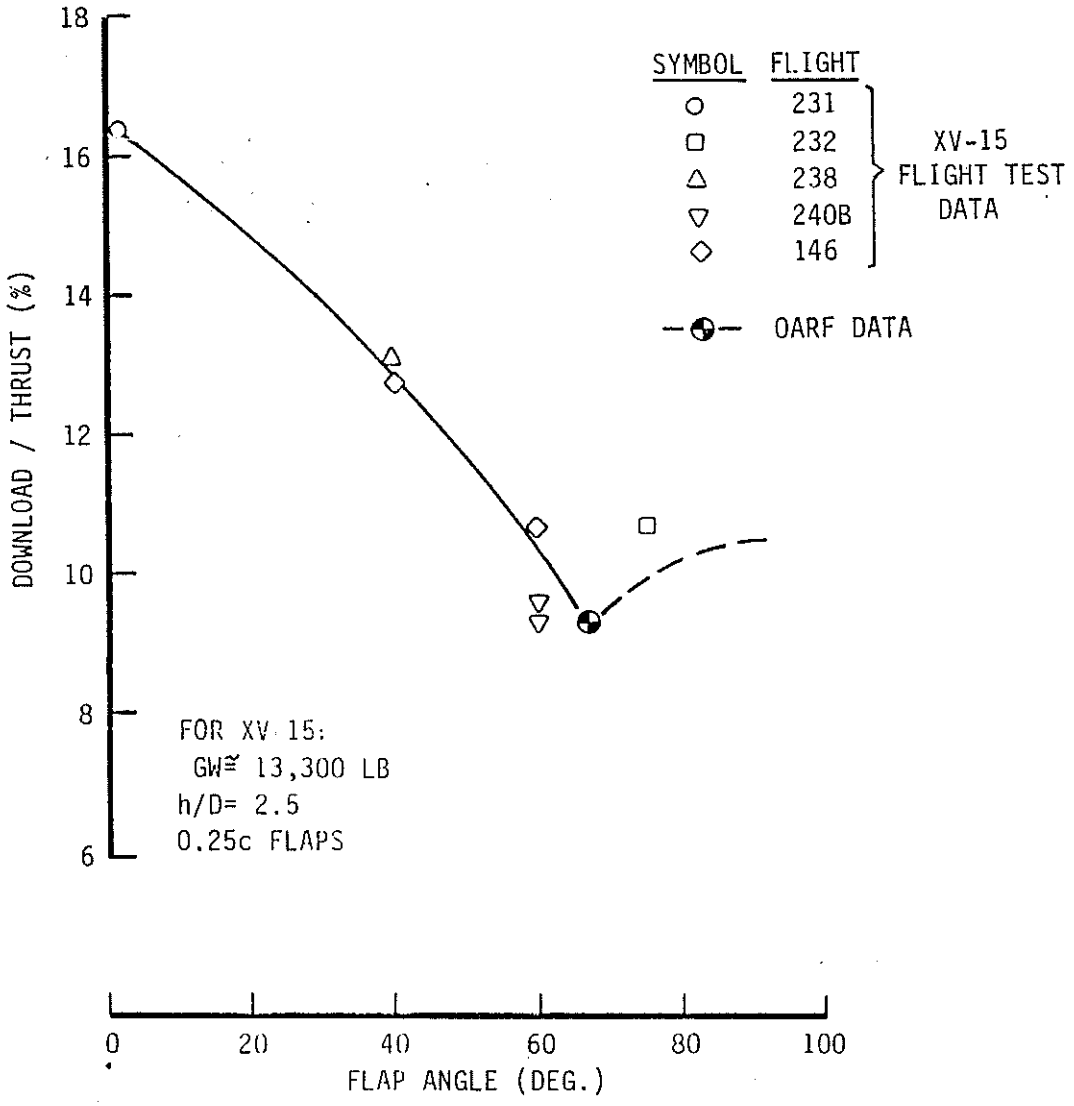

Fig. 19. Effect of Flap Angle on Download/Thrust